Tb^{3+} Luminescence in Tb-Doped and Tb/Gd-Doped $CsCdBr_3$ Crystals: $^5D_4 \rightarrow {}^5D_3$ Cross-Relaxation Rates in Tb^{3+} Pairs

P. Stanley May* and K. Devon Sommer

Department of Chemistry, University of South Dakota, Vermillion, South Dakota 57069

Received: July 7, 1997; In Final Form: October 2, 1997[⊗]

The luminescence properties of Tb^{3+} in $Tb^{3+}-Tb^{3+}$ and $Tb^{3+}-Gd^{3+}$ majority-type pairs in $CsCdBr_3$ are investigated at 77 K and room temperature. $^5D_3 \rightarrow {}^5D_4$ cross-relaxation rates for Tb^{3+} in $Tb^{3+}-Tb^{3+}$ pairs are determined. The intrinsic $^5D_3 \rightarrow {}^5D_4$ and $^5D_3 \rightarrow {}^7F_J$ relaxation rates of Tb^{3+} in the majority-pair site are estimated. The relative numbers of $Tb^{3+}-Tb^{3+}$ and $Tb^{3+}-Gd^{3+}$ pairs in Tb/Gd-doped $CsCdBr_3$ are shown to be consistent with statistical pair formation.

1. Introduction

Despite the large number of investigations of electronic energy transfer processes between metal ions in insulating hosts, there are remarkably few systems for which pairwise transfer rates have been accurately determined. Clearly, pairwise transfer rates could be determined most easily in compounds in which donors and acceptors exist in one type of donor−acceptor pair and individual pairs are well separated. In these systems, there would be only one distinct transfer "event", so that microscopic transfer rates would be directly reflected in the macroscopic luminescence characteristics of the donor population. Currently, the most promising candidates for studies of energy transfer within isolated Ln^{3+} pairs in inorganic insulators are the Ln^{3+}-doped AMX_3 halides, such as $CsMgCl_3$, $CsCdBr_3$, and $CsMgBr_3$. These compounds adopt the hexagonal $CsNiCl_3$ structure, in which the halide ions form infinite chains of face-sharing octahedra running parallel to the c_3 crystal axis. The divalent ions reside at the centers of the octahedra, and the Cs^+ ions lie between the infinite chains. The $[MX_6]^{4-}$ octahedra are slightly elongated along the c_3 axis, so that the site symmetry of the divalent ion is D_{3d}. Trivalent lanthanides are known to enter these lattices predominately as a single type of pair, with each pair substituting for three M^{2+} ions. Henling and McPherson have used EPR to show that the lanthanides are at M^{2+} sites separated by an octahedron with an M^{2+} vacancy.[1,2] The pair can thus be represented as $M^{2+}-Ln^{3+}-(M^{2+}\text{-vacancy})-Ln^{3+}-M^{2+}$. Hereafter, the dominant pair type will be abbreviated as $Ln^{3+}-Ln^{3+}$. The Ln^{3+} environment is similar to that of the unsubstituted M^{2+} ions, except that the Ln^{3+} ions collapse slightly toward the vacancy, lowering the site symmetry to C_{3v}. The Ln^{3+} ions investigated optically in one or more of the $CsMX_3$ hosts include singly doped Pr^{3+},[3−6] Nd^{3+},[7−10] Tb^{3+},[11,12] Ho^{3+},[13,14] Eu^{3+},[15,16] Er^{3+},[17−24] Tm^{3+},[25] and Ce^{3+} [26] systems, and codoped $Tm^{3+}-Pr^{3+}$,[27] $Tm^{3+}-Ho^{3+}$,[28] $Yb^{3+}-Er^{3+}$,[29] $Gd^{3+}-Er^{3+}$ [30] and $Ce^{3+}-Tm^{3+}$ [31] systems. By far, the majority of these spectroscopic investigations of lanthanide pairs in these hosts have centered on upconversion processes, especially in Er^{3+}:$CsCdBr_3$, wherein pair luminescence can be obtained at wavelengths shorter than the excitation wavelength(s).

In this study, the luminescence properties of Tb^{3+} in 0.2%Tb: $CsCdBr_3$ and 1%Gd: 0.1%Tb: $CsCdBr_3$ are used to determine the $^5D_3 \rightarrow {}^5D_4$ cross-relaxation rates in $Tb^{3+}-Tb^{3+}$ pairs at room temperature and 77 K. The observation of $^5D_3 \rightarrow {}^5D_4$ cross-relaxation in Tb-doped $CsCdBr_3$ has been reported previously by Blasse et al.[11,12] The present study extends their work, using spectroscopic data from $Tb^{3+}-Gd^{3+}$ pairs to accurately determine $^5D_3 \rightarrow {}^5D_4$ cross-relaxation rates in $Tb^{3+}-Tb^{3+}$ pairs and the intrinsic $^5D_3 \rightarrow {}^5D_4$ and $^5D_3 \rightarrow {}^7F_J$ relaxation rates. The relative numbers of $Tb^{3+}-Tb^{3+}$ and $Tb^{3+}-Gd^{3+}$ pairs in $CsCdBr_3$ codoped with Tb^{3+} and Gd^{3+} is shown to be consistent with statistical pair formation.

2. Experimental Section

2.1. Synthesis and Crystal Growth. Small crystals of $CsCdBr_3$ were obtained by slow evaporation of solutions of CsBr and cadmium acetate in HBr. 2.6% Tb:$CsCdBr_3$ was prepared by fusing anhydrous $TbBr_3$ with $CsCdBr_3$ in a Vycor ampule under vacuum in a high-temperature oven. A single crystal of 2.6% Tb:$CsCdBr_3$ was then grown from melt via the Bridgman method. The 0.2% Tb:$CsCdBr_3$ was prepared by fusing a small amount of the 2.6% Tb:$CsCdBr_3$ crystal with additional $CsCdBr_3$. The 0.95% Gd:0.11% Tb:$CsCdBr_3$ crystal (hereafter referred to as 1% Gd:0.1% Tb:$CsCdBr_3$) was prepared by fusing the appropriate amounts of 2.6% Tb:$CsCdBr_3$, anhydrous $GdBr_3$ and $CsCdBr_3$. Single crystals of 0.2% Tb:$CsCdBr_3$ and 1% Gd:0.1% Tb:$CsCdBr_3$ were obtained via the Bridgman method. The anhydrous lanthanide bromides were prepared from the lanthanide oxides and ammonium bromide via the so-called "dry route."[32,33] The Tb^{3+} concentration in 2.6% Tb:$CsCdBr_3$ was estimated by dissolving a known amount of the crystal (taken from the center of the boule) in water and comparing the integrated intensities of $Tb^{3+}(^5D_4)$ emissions from this solution with calibration curves of intensity vs Tb^{3+} concentration obtained on standard solutions of $TbBr_3$. Luminescence measurements for concentration determination were performed using a SPEX Fluoromax photon counting spectrophotometer. The lanthanide concentrations given for 0.2% Tb:$CsCdBr_3$ and 1% Gd:0.1% Tb:$CsCdBr_3$ are nominal concentrations, estimated from the weights of the starting materials prior to fusion.

2.2. Spectroscopic Measurements. High-resolution luminescence spectra and time-dependent luminescence data were acquired using a PC-controlled, open-architecture system consisting of nitrogen laser/dye laser excitation (Laser Photonics models UV-12 and DL-14, respectively), a 0.46 M flat-field monochromator (Jobin-Yvon HR460), and a time-resolved photon-counting detection system consisting of a fast, red-sensitive, side-window photomultiplier (Hamamatsu R2949) and a multichannel scaler (Stanford Research SR430). Sample

* Corresponding author. Email: smay@charlie.usd.edu. FAX: (605) 677-6397.

[⊗] Abstract published in *Advance ACS Abstracts,* November 15, 1997.

S1089-5639(97)02199-3 CCC: $14.00

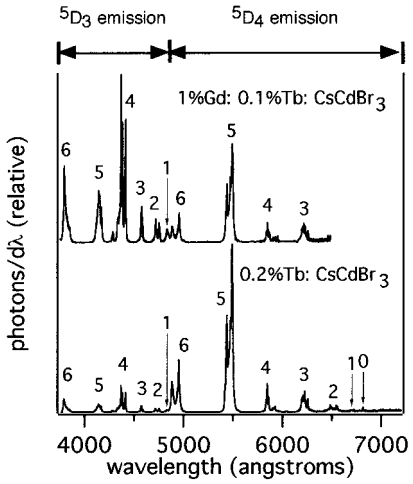

Figure 1. Room-temperature emission spectra of Tb^{3+} in 0.2% Tb:$CsCdBr_3$ and 1% Gd:0.1% Tb:$CsCdBr_3$ (3612 Å excitation/3 Å monochromator resolution).

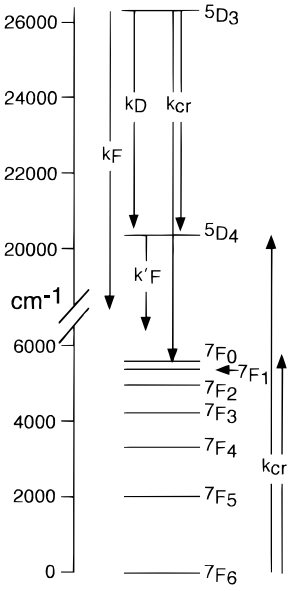

Figure 2. Energy-level diagram of Tb^{3+} in $CsCdBr_3$.

temperatures of 77 K were achieved by immersing the crystals in liquid nitrogen inside a quartz Dewar.

3. Results and Discussion

3.1. Tb^{3+} Luminescence Spectra. The room-temperature luminescence spectra of Tb^{3+} in 0.2% Tb:$CsCdBr_3$ and 1% Gd:0.1% Tb:$CsCdBr_3$ resulting from 361 nm excitation are shown in Figure 1. The spectra have been corrected for monochromator and detector response, such that the integrated intensity of each transition region is proportional to the number of photons emitted in that region following an excitation pulse. An energy-level diagram showing the approximate positions of the $^5D_3$, $^5D_4$, and ^7F_J(J=0→6) multiplet centers in $CsCdBr_3$ is shown in Figure 2. The Tb^{3+} luminescence in Figure 1 is due to transitions from the crystal-field levels of two metastable multiplets, $^5D_3$ and $^5D_4$, down to the crystal-field levels of the ^7F_J(J=0→6) multiplets. For the most part, $^5D_3$ and $^5D_4$ emission appear in distinct spectral regions, the only significant overlap occurring between $^5D_3 \rightarrow {}^7F_0$ and $^5D_4 \rightarrow {}^7F_6$. The transitions in Figure 1 are labeled according to the J value of the ^7F_J multiplet of the corresponding $^5D \rightarrow {}^7F_J$ transition region. Note that $^5D_4$ luminescence corresponding to transitions to all lower lying ^7F_J multiplets are observed in 0.2% Tb:$CsCdBr_3$, although the $^5D_4 \rightarrow {}^7F_1$ and $^5D_4 \rightarrow {}^7F_0$ emissions are quite weak.

A portion of the 0.2% Tb: $CsCdBr_3$ room temperature spectrum has been reported previously by Lammers and Blasse[11] and appears to be identical with that shown in Figure 1. As will be discussed in section 3.3, luminescence decay measurements indicate that $^5D_4$ emission in 0.2% Tb:$CsCdBr_3$ is due almost completely to Tb^{3+} ions belonging to pairs of the type $Tb^{3+}-(Cd^{2+}$ vacancy$)-Tb^{3+}$, whereas ∼40% of the $^5D_3$ emission is due to the small percentage of Tb^{3+} ions which are present in the lattice as single ions. The poor quantum efficiency of $^5D_3$ emission from $Tb^{3+}-Tb^{3+}$ pairs is due to a $^5D_3 \rightarrow {}^5D_4$ cross-relaxation process which depopulates $^5D_3$ in favor of $^5D_4$. Therefore, $^5D_4$ emission dominates the spectrum of Tb^{3+} pairs when exciting into or directly above the $^5D_3$ multiplet, such that approximately five times as many photons are emitted from $^5D_4$ relative to $^5D_3$.[34]

The Tb^{3+} luminescence spectrum for 1% Gd:0.1% Tb:$CsCdBr_3$ (Figure 1) shows a reversal in the relative intensities of $^5D_4$ and $^5D_3$ emission compared to that for 0.2% Tb:$CsCdBr_3$. The majority of Tb^{3+} ions in this lattice are paired with Gd^{3+} ions, which do not deactivate $^5D_3$ emission in favor of $^5D_4$. Luminescence decay measurements indicate that $^5D_3$ emission is due almost entirely to $Tb^{3+}-Gd^{3+}$ pairs, whereas more than half of $^5D_4$ emission intensity (∼56%) is due to the small percentage of Tb^{3+} ions present in $Tb^{3+}-Tb^{3+}$ pairs (see section 3.6). $^5D_4$ emission from $Tb^{3+}-Tb^{3+}$ pairs can compete with that from $Tb^{3+}-Gd^{3+}$ pairs, even though there are ∼17 times as many $Tb^{3+}-Gd^{3+}$ pairs (see section 3.8), because cross-relaxation more effectively populates the $^5D_4$ levels in $Tb^{3+}-Tb^{3+}$ pairs. Whereas five to six times as many photons are emitted from $^5D_4$ relative to $^5D_3$ in $Tb^{3+}-Tb^{3+}$ pairs,[34] the ratio in $Tb^{3+}-Gd^{3+}$ pairs is 0.08−0.09.[35] In contrast, $^5D_3$ emission from $Tb^{3+}-Tb^{3+}$ pairs does not compete with that from $Tb^{3+}-Gd^{3+}$ pairs in 1% Gd:0.1% Tb:$CsCdBr_3$ because of the relatively low concentration of $Tb^{3+}-Tb^{3+}$ pairs *and* the poor quantum efficiency of $^5D_3$ emission from these pairs.

We have also measured the 77 K luminescence spectra of Tb^{3+} in 0.2% Tb:$CsCdBr_3$ and 1% Gd:0.1% Tb:$CsCdBr_3$, and they appear qualitatively similar to the corresponding room-temperature spectra shown in Figure 1 in terms of the $^5D_4$ to $^5D_3$ intensity ratios.

Finally, we note that our luminescence data indicate that, as expected, the crystal-field energy-level structure of Tb^{3+} is essentially identical in $Tb^{3+}-Tb^{3+}$ and $Tb^{3+}-Gd^{3+}$ pairs. The 77 K emission spectra of the $^5D_3 \rightarrow {}^7F_4$ region of Tb^{3+} in 0.2% Tb:$CsCdBr_3$ and 1%Gd:0.1% Tb:$CsCdBr_3$ are shown together for comparison in Figure 3. The peak positions and relative intensities are the same in the two compounds, except that some additional small peaks are seen in the 0.2% Tb:$CsCdBr_3$ spectrum, which are probably due to emission from Tb^{3+} single ions (see section 3.3).

3.2. $Tb^{3+}(^5D_3)$ Relaxation in 1% Gd:0.1% Tb:$CsCdBr_3$. Approximately 90% of the Tb^{3+} ions in 1% Gd:0.1% Tb:$CsCdBr_3$ are in $Tb^{3+}-Gd^{3+}$ pairs (see section 3.8). The only relaxation mechanisms available to the $^5D_3$ levels in these pairs are the intrinsic $^5D_3 \rightarrow {}^5D_4$ and $^5D_3 \rightarrow {}^7F_J$ relaxations (illustrated schematically in Figure 2) with rate constants k_D and k_F, respectively. Both transitions are probably largely radiative in nature due to the large number of phonons required to bridge the relevant energy gaps. There is no indication that any additional $^5D_3$ relaxation mechanisms, such as relaxation via a charge-transfer or $4f^{n-1}5d^1$ state, are active.

$Tb^{3+}(^5D_3)$ emission decay curves were acquired at 77 K and room temperature by exciting directly into the $^5D_3$ multiplet.

TABLE 1: Rate Constants for the Relaxation Pathways from the $^5D_3$ and $^5D_4$ Levels in $Tb^{3+}-Tb^{3+}$ Pairs in $CsCdBr_3$ Illustrated in Figure 2

	$(k_F + k_D)/(s^{-1})^a$	$(k_F + k_D + k_{CR})/(s^{-1})^b$	$k_{CR}/(s^{-1})^c$	$k_D/(s^{-1})^d$	$k_F/(s^{-1})^e$	$k'_F/(s^{-1})^f$
room temp	1217 ± 3	6748 ± 85	5531 ± 85	$99 \pm 10/93 \pm 4$	$1118 \pm 10/1124 \pm 5$	885 ± 2
77 K	1188 ± 2	9608 ± 172	8420 ± 172	$63 \pm 7/78 \pm 4$	$1125 \pm 7/1108 \pm 4$	873 ± 1

[a] Total rate constant for $Tb^{3+}(^5D_3)$ relaxation in $Tb^{3+}-Gd^{3+}$ pairs, determined from $^5D_3$ emission decay curves in 1% Gd:0.1%Tb:$CsCdBr_3$ (see section 3.2). [b] Total rate constant for $Tb^{3+}(^5D_3)$ relaxation in $Tb^{3+}-Tb^{3+}$ pairs, determined from $^5D_3$ emission decay curves in 0.2%Tb:$CsCdBr_3$ (see section 3.3). [c] Rate constant for $^5D_3 \rightarrow {}^5D_4$ cross-relaxation in $Tb^{3+}-Tb^{3+}$ pairs, determined from the difference in the first two columns of the table (see section 3.4) [d] Rate constant for the intrinsic $^5D_3 \rightarrow {}^5D_4$ relaxation pathway of Tb^{3+} in $CsCdBr_3$. The first value listed was calculated as described in section 3.7. The second value was calculated as described in section 3.8. [e] Rate constant for the $^5D_3 \rightarrow {}^5F_J$ relaxation pathways of Tb^{3+} in $CsCdBr_3$, calculated from the difference in the first and fourth columns of the table. [f] Total rate constant for $Tb^{3+}(^5D_4)$ relaxation in $CsCdBr_3$, determined from $^5D_4$ emission decay curves following direct excitation into $^5D_4$ (see section 3.5).

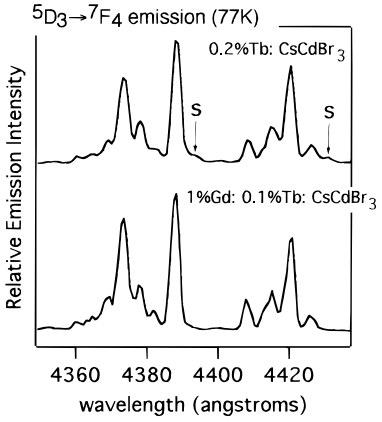

Figure 3. 77 K emission spectra of the $^5D_3 \rightarrow {}^7F_4$ region of Tb^{3+} in 0.2% Tb:$CsCdBr_3$ and 1% Gd:0.1% Tb:$CsCdBr_3$. Peaks marked with "s" in the 0.2% Tb:$CsCdBr_3$ spectrum indicate emission from Tb^{3+} single ions.

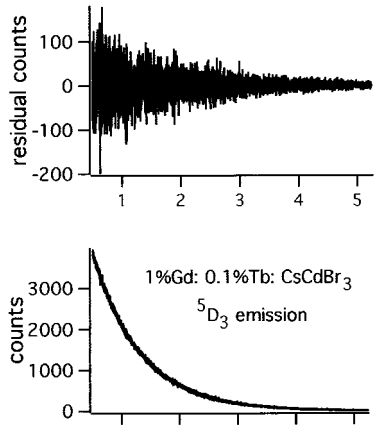

Figure 4. (Lower) Room-temperature decay curve for $Tb^{3+}(^5D_3)$ luminescence in 1% Gd:0.1% Tb:$CsCdBr_3$ obtained using direct excitation into $^5D_3$ at 3796 Å, monitoring $^5D_3 \rightarrow {}^7F_4$ emission at 4583 Å. (Upper) Residuals of fit to an exponential function (see section 3.2). Residual counts = experiment − theory.

The decay curves displayed a weak, short-lived component, due in part to emission from $Tb^{3+}-Tb^{3+}$ pairs, and a stronger, longer-lived component due to emission from $Tb^{3+}-Gd^{3+}$ pairs. The curves are almost perfectly exponential from ~0.5 ms following the excitation pulse, and these portions of the curves were fit to an exponential function to obtain $^5D_3$ relaxation-rate constants of $(k_D + k_F) = 1217 \pm 3\ s^{-1}$ at room temperature and $(k_D + k_F) = 1188 \pm 2\ s^{-1}$ at 77 K (see Table 1). A room-temperature $^5D_3$ decay curve obtained by exciting at 379.6 nm and monitoring $^5D_3$ emission at 437.3 nm is shown in Figure 4, together with the residuals resulting from a fit to an exponential function. The excellent residuals strongly suggest that emission from only one type of Tb^{3+} species is being monitored.

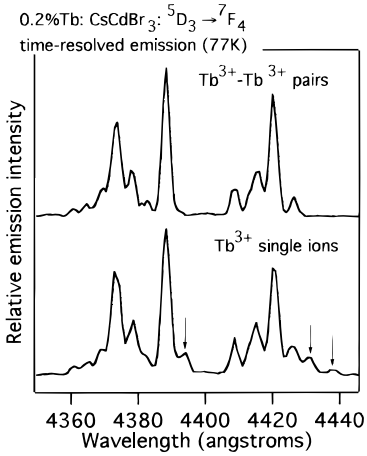

Figure 5. Time-resolved emission spectra of the $^5D_3 \rightarrow {}^7F_4$ region of Tb^{3+} in 0.2% Tb:$CsCdBr_3$ using 3799 Å excitation. (Lower spectrum) Single-ion spectrum acquired using a time window of 205−1800 μs following pulsed excitation. Peaks not seen in the pair spectrum are marked with arrows. (Upper spectrum) $Tb^{3+}-Tb^{3+}$ pair spectrum acquired using a time window of 13−204 μs following pulsed excitation, subtracting out the long-lived single-ion component.

3.3. $Tb^{3+}(^5D_3)$ Relaxation in 0.2% Tb:$CsCdBr_3$. The vast majority of Tb^{3+} ions in 0.2% Tb:$CsCdBr_3$ are in $Tb^{3+}-Tb^{3+}$ pairs, although a small percentage of Tb^{3+} single ions are also present. In addition to the intrinsic $^5D_3 \rightarrow {}^5D_4$ and $^5D_3 \rightarrow {}^7F_J$ relaxation mechanisms active in $Tb^{3+}-Gd^{3+}$ pairs, a $^5D_3 \rightarrow {}^5D_4$ cross-relaxation process (illustrated in Figure 2) is also active in depopulating $^5D_3$. Since cross relaxation occurs between Tb^{3+} ions at a single, fixed $Tb^{3+}-Tb^{3+}$ separation, the process can be described in terms of a single rate constant, k_{CR}. Therefore, the total rate constant for $Tb^{3+}(^5D_3)$ relaxation is given by $k_D + k_F + k_{CR}$ (see Figure 2).

$Tb^{3+}(^5D_3)$ emission decay curves were acquired at 77 K and room temperature by exciting directly into the $^5D_3$ multiplet (379.6 nm at room temperature, 379.9 nm at 77 K). The decay curves displayed a strong, short-lived component, due to emission from $Tb^{3+}-Tb^{3+}$ pairs, and a weaker, longer-lived component due to emission from Tb^{3+} single ions. To establish that the longer-lived emission is indeed due to Tb^{3+}, we acquired time-resolved 77 K emission spectra of the $^5D_3 \rightarrow {}^7F_4$ region, using a time window of 13−204 μs after excitation to obtain the spectrum of the short-lived luminescence and a time window of 205−1800 μs to obtain the spectrum of the long-lived component. These spectra are shown in Figure 5. The long-lived contribution to the 13−204 μs spectrum has been subtracted out of the top spectrum in Figure 5, so that the luminescence shown is due entirely to $Tb^{3+}-Tb^{3+}$ pairs. Obviously, both the short- and long-lived emissions are due to Tb^{3+} ions in similar crystal-field environments, although some additional weak peaks are seen in the single-ion spectrum. These additional peaks are marked with arrows in Figure 5.

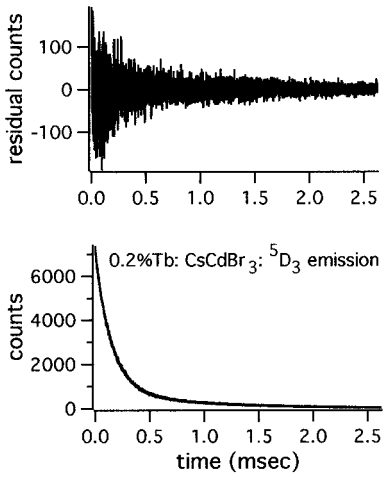

Figure 6. (Lower) Room-temperature decay curve for $Tb^{3+}(^5D_3)$ luminescence in 0.2% Tb:$CsCdBr_3$ obtained using direct excitation into $^5D_3$ at 3796 Å, monitoring $^5D_3 \rightarrow {}^7F_4$ emission at 4373 Å. (Upper) Residuals of fit to eq 1 (see section 3.3). Residual counts = experiment − theory.

To obtain the $^5D_3$ relaxation rates in $Tb^{3+}-Tb^{3+}$ pairs and Tb^{3+} single ions, the decay curves were fit to

$$I(t) = I^0_{\text{pairs}}\, e^{-(k_{CR} + k_D + k_F)t} + I^0_{\text{single}}\, e^{-(k_D + k_F)t} \qquad (1)$$

where $I(t)$ is $^5D_3$ emission intensity as a function of time and I^0_{pairs} and I^0_{single} are the intensities due to $Tb^{3+}-Tb^{3+}$ pairs and Tb^{3+} single ions, respectively, at $t = 0$. Four parameters were allowed to vary in the fits: I^0_{pairs}, I^0_{single}, $(k_{CR} + k_D + k_F)$, and $(k_D + k_F)$. A room-temperature $^5D_3$ decay curve obtained by exciting at 379.6 nm and monitoring $^5D_3$ emission at 437.3 nm is shown in Figure 6, together with the residuals resulting from a fit to eq 1. The excellent residuals support our assumption that there are only two types of $Tb^{3+}(^5D_3)$ emittors present in significant concentrations. The rate constants for $^5D_3$ relaxation in $Tb^{3+}-Tb^{3+}$ pairs were determined to be $(k_{CR} + k_D + k_F) = 6748 \pm 85\ s^{-1}$ at room temperature and $(k_{CR} + k_D + k_F) = 9608 \pm 172\ s^{-1}$ at 77 K (see Table 1). The rate constants for $^5D_3$ relaxation in Tb^{3+} single ions were determined to be $(k_D + k_F) = 1199 \pm 25\ s^{-1}$ at room temperature and $(k_D + k_F) = 1126 \pm 16\ s^{-1}$ at 77 K.

The results of our fits to eq 1 can also be used to estimate the fraction of $^5D_3$ emission intensity due to single ions. Integrating eq 1 to obtain the total integrated emission intensity following an excitation pulse, $\int_0^\infty I(t)$, yields

$$\int_0^\infty I(t) = \frac{I^0_{\text{pairs}}}{(k_{CR} + k_D + k_F)} + \frac{I^0_{\text{single}}}{(k_D + k_F)} \qquad (2)$$

where the first term on the right-hand side of the equation represents the integrated intensity from pairs and the second term corresponds to the integrated intensity from single ions. The fraction of the integrated emission due to single ions, $\int_0^\infty I_{\text{single}}(t)/\int_0^\infty I(t)$, is, therefore, given by

$$\frac{\int_0^\infty I_{\text{single}}(t)}{\int_0^\infty I(t)} = \frac{I^0_{\text{single}}(k_{CR} + k_D + k_F)}{I^0_{\text{single}}(k_{CR} + k_D + k_F) + I^0_{\text{pairs}}(k_D + k_F)} \qquad (3)$$

From the fits to eq 1, $I^0_{\text{pairs}} = (8.0 \pm 0.2)\cdot I^0_{\text{single}}$ at room temperature. So, by substituting for I^0_{pairs} in eq 3, and using the fitted room-temperature values of $(k_{CR} + k_D + k_F)$ and $(k_D + k_F)$, we obtain $\int_0^\infty I_{\text{single}}(t)/\int_0^\infty I(t) = 0.41$, meaning that approximately 40% of $^5D_3$ emission is due to Tb^{3+} single ions at room temperature (379.6 nm excitation).

The ratio of the initial population of excited Tb^{3+} single ions to excited Tb^{3+} ions in pairs, $n^0_{\text{single}}/n^0_{\text{pairs}}$, following excitation is given by

$$\frac{n^0_{\text{single}}}{n^0_{\text{pairs}}} = \frac{I^0_{\text{single}}}{I^0_{\text{pairs}}} \cdot \frac{(k_D + k_F)}{(k_{CR} + k_D + k_F)} \qquad (4)$$

Using the fitted values of $I^0_{\text{single}}/I^0_{\text{pairs}}$, $(k_{CR} + k_D + k_F)$, and $(k_D + k_F)$ for our room-temperature data, we obtain $n^0_{\text{single}}/n^0_{\text{pairs}} = 2.22 \times 10^{-2} \pm 0.08 \times 10^{-2}$. Therefore, ~2% of the excited Tb^{3+} ions produced with 379.6 nm excitation are Tb^{3+} single ions. To the extent that Tb^{3+} single ions and Tb^{3+} ions in $Tb^{3+}-Tb^{3+}$ pairs are excited with equal efficiency, this implies that ~2% of the Tb^{3+} ions in 0.2%Tb:$CsCdBr_3$ are present as single ions. This is consistent with the results of Berdowski et al., who estimate that ~5% of the Tb^{3+} in their sample of 0.2%Tb:$CsCdBr_3$ exist as single ions.[12]

3.4. $^5D_3 \rightarrow {}^5D_4$ Cross-Relaxation Rates in $Tb^{3+}-Tb^{3+}$ pairs. The rate constant, k_{CR}, for cross-relaxation in $Tb^{3+}-Tb^{3+}$ pairs can be calculated from the difference in the measured $^5D_3$ relaxation rates in $Tb^{3+}-Tb^{3+}$ pairs and $Tb^{3+}-Gd^{3+}$ pairs, since $(k_{CR} + k_D + k_F) - (k_D + k_F) = k_{CR}$. At room temperature, $(k_{CR} + k_D + k_F) = 6748 \pm 85\ s^{-1}$ (section 3.3) and $(k_D + k_F) = 1217 \pm 3\ s^{-1}$ (section 3.2), which implies a cross-relaxation rate constant of $k_{CR} = 5531 \pm 85\ s^{-1}$. At 77 K, $(k_{CR} + k_D + k_F) = 9608 \pm 172\ s^{-1}$ (section 3.3) and $(k_D + k_F) = 1188 \pm 2\ s^{-1}$ (section 3.2), which implies a cross-relaxation rate constant of $k_{CR} = 8420 \pm 172\ s^{-1}$ (see Table 1).

Henling and McPherson have shown that the $Gd^{3+}-Gd^{3+}$ separation in Gd^{3+}-doped $CsCdBr_3$ decreases from 6.03 Å at room temperature to 5.93 Å at 77 K.[2] The maximum effect of this decrease for a Förster−Dexter type multipole mechanism, however, would be an 18% increase in the transfer rate (quadrupole−quadrupole mechanism), whereas the observed increase is ~52%. Berdowski et al. have suggested that the cross-relaxation mechanism may involve donor and/or acceptor transitions originating from mid-lying crystal-field levels of the $^5D_3$ and/or $^7F_6$ multiplets, such that the increase in the cross-relaxation rate upon cooling from room temperature to 77 K is due mainly to increasing the thermal populations of these levels at the expense of higher-lying levels.[12] This explanation is consistent with the fact that the cross relaxation rate *decreases* upon further cooling from 77 K. However, the energy mismatch between the donor and acceptor transitions is not yet precisely known, so that the temperature dependence may be affected by phonon-assisted processes.

3.5. $Tb^{3+}(^5D_4)$ Emission Dynamics in 0.2% Tb:$CsCdBr_3$. $Tb^{3+}(^5D_4)$ luminescence in 0.2% Tb: $CsCdBr_3$ following excitation into the $^5D_3$ manifold is due almost entirely to $Tb^{3+}-Tb^{3+}$ pairs. No contribution from Tb^{3+} single ions is observed, which is not surprising, given the small percentage of Tb^{3+} present as single ions and the fact that the majority of Tb^{3+} single ions relax directly to the ^7F_J levels, bypassing $^5D_4$. The rate of change in the population of $Tb^{3+}(^5D_4)$ with time is, therefore, given by

$$\frac{\partial n_4}{\partial t} = (k_{CR} + k_D)\cdot n_3 - k'_F \cdot n_4 \qquad (5)$$

where n_3 and n_4 are the populations of $^5D_3$ and $^5D_4$, respectively,

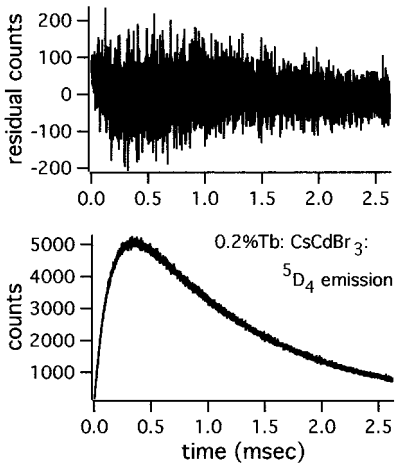

Figure 7. (Lower) Time dependence of $Tb^{3+}(^5D_4)$ luminescence in 0.2% Tb:$CsCdBr_3$ following excitation into $^5D_3$ at 3796 Å, monitoring $^5D_3 \rightarrow {}^7F_4$ emission at 5493 Å. (Upper) Residuals of fit to eq 7 (see section 3.5). Residual counts = experiment − theory.

and k'_F is the rate constant for $^5D_4 \rightarrow {}^7F_J$ relaxation (see Figure 2). Solving eq 5 for n_4 as a function of time gives

$$n_4 = \frac{n_3^0(k_{CR} + k_D)}{(k_{CR} + k_D + k_F) - k'_F}(e^{-k'_F t} - e^{-(k_{CR} + k_D + k_F)t}) \quad (6)$$

The time-dependence of $^5D_4$ luminescence following $^5D_3$ excitation is, therefore, given by

$$I(^5D_4) = Ke^{-k'_F t} - Ke^{-(k_{CR} + k_D + k_F)t} \quad (7)$$

where K is a constant which is proportional to $\{n_3^0(k_{CR} + k_D)\}/\{(k_{CR} + k_D + k_F) - k'_F\}$. The first term in eq 7 corresponds to the depopulation of $^5D_4$ via $^5D_4 \rightarrow {}^7F_J$, and the second term corresponds to the feeding of the $^5D_4$ levels via $^5D_3 \rightarrow {}^5D_4$ (see Figure 2).

$I(^5D_4)$ vs time data following excitation into or immediately above $^5D_3$ was fit to eq 7, using K, k'_F, and $(k_{CR} + k_D + k_F)$ as adjustable parameters. Fits to the room-temperature data yielded $k'_F = 884 \pm 5\ s^{-1}$ and $(k_{CR} + k_D + k_F) = 6920 \pm 38\ s^{-1}$. The fitted value of k'_F compares well with the value of $885 \pm 2\ s^{-1}$ determined from the exponential $^5D_4$ decay curves obtained by exciting directly into $^5D_4$. While the fitted value of $(k_{CR} + k_D + k_F)$ is slightly larger than the value of $6748 \pm 85\ s^{-1}$ obtained from the $Tb(^5D_3)$ decay curves in 0.2% Tb:$CsCdBr_3$ (see section 3.3), it is nonetheless clear that eq 7 is an adequate description of the evolution of $Tb(^5D_4)$ luminescence in 0.2% Tb:$CsCdBr_3$. The faster-than-expected $^5D_4$ rise is probably due to a small contribution from tightly coupled pairs, in which Tb^{3+} ions occupy adjacent Cd^{2+} positions in the lattice. Such pairs have been observed for other lanthanides in $CsCdBr_3$.[8] The fact that $^5D_3$ emission from such pairs is not readily evident is not suprising, since the efficient $^5D_3 \rightarrow {}^5D_4$ cross-relaxation expected in such pairs would largely quench $^5D_3$ emission.

A sample fit of eq 7 to room-temperature $^5D_4$ emission vs time is shown in Figure 7, together with the residuals of the fit. The residuals testify to the general excellence of the fits, with the exception of a small positive deviation at early times, corresponding to a fast component in the rise. Again, such a component would be consistent with the fast rise expected for tightly bound $Tb^{3+}-Tb^{3+}$ pairs.

Fits to 77 K data yielded $k'_F = 852 \pm 7\ s^{-1}$ and $(k_{CR} + k_D + k_F) = 10\ 100 \pm 10\ s^{-1}$, which compare reasonably well to the values of $(k_{CR} + k_D + k_F) = 9608 \pm 172\ s^{-1}$, determined from $^5D_3$ emission (see section 3.3), and $k'_F = 873 \pm 1\ s^{-1}$, determined from $^5D_4$ emission following direct $^5D_4$ excitation. As with the room-temperature data, the values obtained from fits to eq 7 are somewhat skewed by a small fast component to the rise. The residuals of the fits to the 77 K data are similar to those shown for the room temperature data in Figure 7 and show an early positive deviation.

3.6. $Tb^{3+}(^5D_4)$ Emission Dynamics in 1% Gd:0.1% Tb:$CsCdBr_3$. Upon $^5D_3$ excitation in 1% Gd:0.1% Tb:$CsCdBr_3$, significant $^5D_4$ emission from both $Tb^{3+}-Tb^{3+}$ and $Tb^{3+}-Gd^{3+}$ pairs is observed. The rate of change in the entire $Tb^{3+}(^5D_4)$ population with time is, therefore, given by

$$\frac{\partial n_4}{\partial t} = (k_{CR} + k_D)\cdot n_3^{Tb-Tb} + k_D \cdot n_3^{Tb-Gd} - k'_F \cdot n_4 \quad (8)$$

where n_3^{Tb-Tb} is the $Tb^{3+}(^5D_3)$ population in $Tb^{3+}-Tb^{3+}$ pairs and n_3^{Tb-Gd} is the $Tb^{3+}(^5D_3)$ population in $Tb^{3+}-Gd^{3+}$ pairs. Solving eq 8 for n_4 as a function of time gives

$$n_4 = \frac{n_3^{Tb-Tb(0)}(k_{CR} + k_D)}{(k_{CR} + k_D + k_F) - k'_F}(e^{-k'_F t} - e^{-(k_{CR} + k_D + k_F)t}) + \frac{n_3^{Tb-Gd(0)}k_D}{(k_D + k_F) - k'_F}(e^{-k'_F t} - e^{-(k_D + k_F)t}) \quad (9)$$

where $n_3^{Tb-Tb(0)}$ is the initial $Tb^{3+}(^5D_3)$ population in $Tb^{3+}-Tb^{3+}$ pairs, and $n_3^{Tb-Gd(0)}$ is the initial $Tb^{3+}(^5D_3)$ population in $Tb^{3+}-Gd^{3+}$ pairs.

The time-dependence of $^5D_4$ luminescence following $^5D_3$ excitation is, therefore, given by

$$I(^5D_4) = K(e^{-k'_F t} - e^{-(k_{CR} + k_D + k_F)t}) + K'(e^{-k'_F t} - e^{-(k_D + k_F)t}) \quad (10)$$

where K is a constant proportional to $\{n_3^{Tb-Tb(0)}(k_{CR} + k_D)\}/\{(k_{CR} + k_D + k_F) - k'_F\}$, and K' is a constant proportional to $\{n_3^{Tb-Gd(0)}k_D\}/\{(k_D + k_F) - k'_F\}$. The first term in eq 10 corresponds to emission from $Tb^{3+}-Tb^{3+}$ pairs, and the second to emission from $Tb^{3+}-Gd^{3+}$ pairs.

The $I(^5D_4)$ vs time data was fit to eq 10 by treating K and K' as adjustable parameters, and fixing the values of k'_F, $(k_{CR} + k_D + k_F)$, and $(k_D + k_F)$ to those given in Table 1. A fit of eq 10 to room-temperature $^5D_4$ emission vs time is shown in Figure 8, together with the residuals of the fit. The near-perfect residuals strongly support our description of $^5D_4$ emission following $^5D_3$ excitation in 1% Gd:0.1% Tb:$CsCdBr_3$. Fits to the 77 K data are of comparable quality.

Equation 10 can be integrated with respect to time to determine the relative contributions from $Tb^{3+}-Tb^{3+}$ and $Tb^{3+}-Gd^{3+}$ pairs to $^5D_4$ emission, since the first and second terms of eq 10 correspond to emission from $Tb^{3+}-Tb^{3+}$ and $Tb^{3+}-Gd^{3+}$ pairs, respectively. At room temperature, $Tb^{3+}-Tb^{3+}$ pairs account for ~56% of $^5D_4$ emission in 1% Gd:0.1% Tb:$CsCdBr_3$, even though there are ~8.6 times as many $Tb^{3+}-Gd^{3+}$ pairs (see section 3.8).

3.7. Estimation of the Intrinsic $^5D_3 \rightarrow {}^5D_4$ and $^5D_3 \rightarrow {}^7F_J$ Relaxation Rates of Tb^{3+} in Majority Pair Sites. The intrinsic $^5D_3 \rightarrow {}^5D_4$ and $^5D_3 \rightarrow {}^7F_J$ relaxation rates of Tb^{3+} in majority-pair sites can be estimated by comparing the ratio of $^5D_4$ to $^5D_3$

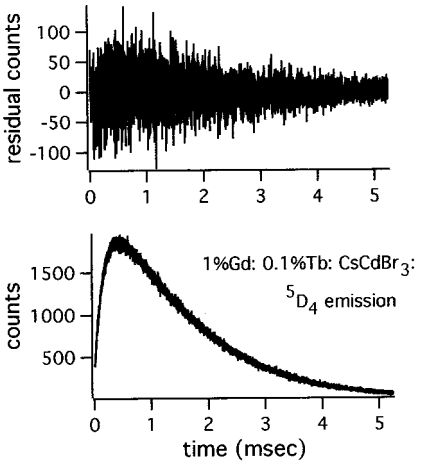

Figure 8. (Lower) Time dependence of $Tb^{3+}(^5D_4)$ luminescence in 1%Gd:0.1% Tb:$CsCdBr_3$ following excitation into $^5D_3$ at 3796 Å, monitoring $^5D_3 \rightarrow {}^7F_4$ emission at 5490 Å. (Upper) Residuals of fit to eq 10 (see section 3.6). Residual counts = experiment − theory.

emission intensity from $Tb^{3+}-Tb^{3+}$ pairs to that from $Tb^{3+}-Gd^{3+}$ pairs. The $^5D_4$-to-$^5D_3$ intensity ratio, I_R, is given by

$$I_R^{Tb-Tb} = \text{const.} \times \frac{(k_{CR} + k_D)}{k_F} \tag{11}$$

for $Tb^{3+}-Tb^{3+}$ pairs and by

$$I_R^{Tb-Gd} = \text{const.} \times \frac{k_D}{k_F} \tag{12}$$

for Tb^{3+}-Gb^{3+} pairs. The proportionality constants in eqs 11 and 12 are the same, as long as the intrinsic $^5D_3$ and $^5D_4$ relaxation processes are identical in $Tb^{3+}-Tb^{3+}$ and $Tb^{3+}-Gd^{3+}$ pairs. Therefore

$$\frac{I_R^{Tb-Tb}}{I_R^{Tb-Gd}} = \frac{(k_{CR} + k_D)}{k_D} \tag{13}$$

which can be rearranged to give

$$k_D = k_{CR} \cdot \left[\frac{I_R^{Tb-Tb}}{I_R^{Tb-Gd}} - 1\right]^{-1} \tag{14}$$

The values of I_R^{Tb-Tb} and I_R^{Tb-Gd} were determined from the luminescence spectra of 0.2% Tb:$CsCdBr_3$ and 1% Gd:0.1%Tb:$CsCdBr_3$, respectively, after taking into account the contributions to $^5D_3$ emission from Tb^{3+} single ions in the 0.2% Tb:$CsCdBr_3$ spectra and the contributions to $^5D_4$ emission from $Tb^{3+}-Tb^{3+}$ pairs in the 1% Gd:0.1% Tb:$CsCdBr_3$ spectra. Note that the accuracy of k_D is not affected by corrections to the emission spectra for monochromator response, etc., because such correction factors will cancel in the ratio I_R^{Tb-Tb}/I_R^{Tb-Gd}.

Using eq 14, the values for k_{CR} in Table 1, and the values of $I_R^{Tb-Tb}/I_R^{Tb-Gd} = 57$ at room temperature and $I_R^{Tb-Tb}/I_R^{Tb-Gd} = 135$ at 77 K, determined as described above, we calculate $k_D = 99 \pm 10\ s^{-1}$ at room temperature and $k_D = 63 \pm 7\ s^{-1}$ at 77 K (see Table 1). Unfortunately, it is difficult to estimate the uncertainties in the values of I_R^{Tb-Tb}/I_R^{Tb-Gd} and, therefore, in the calculated values of k_D. The uncertainties given for k_D are the probable errors calculated assuming a 10% error in our values of I_R^{Tb-Tb}/I_R^{Tb-Gd}.

3.8. Determination of Relative Numbers of $Tb^{3+}-Gd^{3+}$ and $Tb^{3+}-Tb^{3+}$ Pairs in 1%Gd:0.1%Tb:$CsCdBr_3$. The results of the fits to $I(^5D_4)$ vs time data in section 3.6 can be used to estimate the relative numbers of $Tb^{3+}-Gd^{3+}$ and $Tb^{3+}-Tb^{3+}$ pairs in 1% Gd:0.1% Tb:$CsCdBr_3$. The ratio of the fit parameters K' to K is given by

$$\frac{K'}{K} = \frac{[n_3^{Tb-Gd(0)} k_D]}{[(k_D + k_F) - k_F']} \cdot \left[\frac{[n_3^{Tb-Tb(0)}(k_{CR} + k_D)]}{[(k_{CR} + k_D + k_F) - k_F']}\right]^{-1} \tag{15}$$

which can be rearranged to obtain

$$\frac{n_3^{Tb-Gd(0)}}{n_3^{Tb-Tb(0)}} = \frac{K'}{K} \cdot \frac{[(k_D + k_F) - k_F']}{[k_D]} \cdot \frac{[(k_{CR} + k_D)]}{[(k_{CR} + k_D + k_F) - k_F']} \tag{16}$$

Using eq 16, the rate constants in Table 1, and the values of K'/K obtained from the fits described in section 3.6 ($K'/K = 2.5 \pm 0.1$ room temperature; $K'/K = 2.2 \pm 0.1$, 77 K), we obtain $n_3^{Tb-Gd(0)}/n_3^{Tb-Tb(0)} = 8.0 \pm 0.9$ and $n_3^{Tb-Gd(0)}/n_3^{Tb-Tb(0)} = 10.7 \pm 1.4$ from the room temperature and 77 K data, respectively. Taking into account that there are twice as many Tb^{3+} ions in a $Tb^{3+}-Tb^{3+}$ pair compared to a $Tb^{3+}-Gd^{3+}$ pair, the room temperature data imply that the ratio of $Tb^{3+}-Gd^{3+}$ to $Tb^{3+}-Tb^{3+}$ pairs is 16 ± 2, while the 77 K data implies this ratio is 21 ± 3. If the lanthanides form pairs in a purely statistical manner, with no preference being given to the formation of a particular pair type, one would expect the ratio of $Tb^{3+}-Gd^{3+}$ to $Tb^{3+}-Tb^{3+}$ pairs to be ~17. Therefore, although the discrepancy between the room temperature and 77 K results indicate a reasonably large uncertainty in our determination of the pair ratios, the data support statistics as the main driving force for pair formation.

If the statistical value of $n_3^{Tb-Gd(0)}/n_3^{Tb-Tb(0)} = 8.6$ is assumed, eq 16 can also be rearranged to solve for k_D.

$$k_D = k_{CR} \cdot \left[\frac{K'}{K} \cdot \frac{(k_D + k_F) - k_F'}{(k_{CR} + k_D + k_F) - k_F'}\right] \cdot \left[\frac{n_3^{Tb-Gd(0)}}{n_3^{Tb-Tb(0)}} - \frac{K'}{K} \cdot \frac{(k_D + k_F) - k_F'}{(k_{CR} + k_D + k_F) - k_F'}\right]^{-1} \tag{17}$$

Using eq 17, $n_3^{Tb-Gd(0)}/n_3^{Tb-Tb(0)} = 8.6$, the values for K'/K given above, and the values for $(k_{CR} + k_D + k_F)$, $(k_{CR} + k_D + k_F)$, and k_F' in Table 1, we obtain $k_D = 93 \pm 4\ s^{-1}$ at room temperature and $k_D = 78 \pm 4\ s^{-1}$ at 77 K, which compare reasonably well with the values of $99 \pm 10\ s^{-1}$ and $63 \pm 7\ s^{-1}$, respectively, obtained from luminescence intensity data in section 3.7 (see Table 1).

4. Conclusions

Comparison of the spectroscopic properties of Tb^{3+} in $Tb^{3+}-Tb^{3+}$ and $Tb^{3+}-Gd^{3+}$ pairs in $CsCdBr_3$ have enabled the determination of the $^5D_3 \rightarrow {}^5D_4$ cross-relaxation rate constant (in $Tb^{3+}-Tb^{3+}$ pairs), the intrinsic $^5D_3 \rightarrow {}^5D_4$ rate constant, and the $^5D_3 \rightarrow {}^7F_J$ rate constant for Tb^{3+} at room temperature and 77 K. The relative concentrations of the various lanthanide pairs formed by codoping Tb^{3+} and Gd^{3+} into $CsCdBr_3$ is determined by statistical considerations. The energy-level structure and intrinsic $^5D_3$ relaxation dynamics of Tb^{3+} single ions is very similar to that for Tb^{3+} ions in pairs, although some differences are observed in the emission spectra of the two species. Since absolute pairwise transfer rates for the $^5D_3 \rightarrow {}^5D_4$ cross-relaxation process are now known, future work will include a crystal-field energy-level analysis on Tb^{3+} in $CsCdBr_3$ in order to identify the crystal-field levels involved and calculate the multipole−

multiple contributions to transfer. Crystal-field analyses of several other Ln^{3+} ions in $CsCdBr_3$ have appeared in the literature,[3,7,13,15,17,22] and the crystal-field energy parameters appear to vary smoothly across the series.[3] The published parameters, therefore, should be of great utility in performing the Tb^{3+} energy-level analysis and in making crystal-field level assignments.

Acknowledgment. Acknowledgement is made to the donors of the Petroleum Research Fund, administered by the ACS, for partial support of this research.

References and Notes

(1) McPherson, G. L.; Henling, L. M. *Phys. Rev. B* **1977**, *16*, 1889.
(2) Henling, L. M.; McPherson, G. L. *Phys. Rev. B* **1977**, *16*, 4756.
(3) Antic-Fidancev, E.; Lemaitre-Blaise, M.; Chaminade, J. P.; Porcher, P. *J. Alloys Compounds* **1995**, *225*, 95.
(4) Neukum, J.; Bodenschatz, N.; Heber, *J. Phys. Rev. B* **1994**, *50*, 3536.
(5) Schaefer, U.; Neukum, J.; Bodenschatz, N.; Heber, J. *J. Lumin.* **1994**, *60*−*61*, 633.
(6) Heber, J.; Schaefer, U.; Neukum, J.; Bodenschatz, N. *Acta Phys. Pol. A* **1993**, *84*, 889.
(7) Barthem, R. B.; Buisson, R.; Cone, R. L. *J. Chem. Phys.* **1989**, *91*, 627.
(8) Barthou, C.; Barthem, R. B. *J. Lumin.* **1990**, *46*, 9.
(9) Barthem, R. B.; Buisson, R.; Madeore, F.; Vial, J. C.; Chaminade, J. P. *J. Phys.* **1987**, *48*, 379.
(10) Barthem, R. B.; Buisson, R.; Vial, J. C.; Chaminade, J. P. *J. Phys. Colloq.* **1987**, *C7*, 113.
(11) Lammers, M. J. J.; Blasse, G. *Chem. Phys. Lett.* **1986**, *126*, 405.
(12) Berdowski, P. A. M.; Lammers, M. J. J.; Blasse, G. *J. Chem. Phys.* **1985**, *83*, 476.
(13) Mujajii, M.; Jones, G. D.; Syme, R. W. G. *Phys. Rev. B* **1993**, *48*, 710.
(14) Mujaji, M.; Jones, G. D.; Syme, R. W. G. *J. Lumin.* **1992**, *53*, 473.
(15) Pelle, F.; Gardant, N.; Genotelle, M.; Goldner, Ph.; Porcher, P. *J. Phys. Chem. Solids* **1995**, *56*, 1003.
(16) Cockroft, N. J.; Jones, G. D.; Syme, R. W. G. *J. Lumin.* **1989**, *43*, 275.
(17) Quagliano, J. R.; Cockroft, N. J.; Gunde, K. E.; Richardson, F. S. *J. Chem. Phys.*, in press.
(18) Pelle, F.; Goldner, Ph. *Opt. Mater.* **1994**, *4*, 121.
(19) Bordallo, H. N.; Barthem, R. B.; Barthou, C. *Solid State Commun.* **1994**, *92*, 721.
(20) Pelle, F.; Goldner, Ph. *Phys. Rev. B* **1993**, *48* 9995.
(21) McPherson, G. L.; Gharavi, A.; Meyerson, S. L. *Chem. Phys.* **1992**, *165*, 361.
(22) Cockroft, N. J.; Jones, G. D.; Nguyen, D. C. *Phys. Rev. B* **1992**, *45*, 5187.
(23) McPherson, G. L.; Meyerson, S. L. *Chem. Phys. Lett.* **1991**, *179*, 325.
(24) McPherson, G. L.; Meyerson, S. L. *Chem. Phys. Lett.* **1990**, *167*, 471.
(25) Gharavi, A.; McPherson, G. L. *Chem. Phys. Lett.* **1992**, *200*, 279.
(26) Blasse, G.; Wolfert, A.; McPherson, G. L. *J. Solid State Chem.* **1985**, *57*, 396.
(27) Murdoch, K. M.; Cockroft, N. J. *Phys. Rev. B* **1996**, *54*, 4589.
(28) Bodenschatz, N.; Neukum, J.; Heber, J. *J. Lumin.* **1996**, *66*−*67*, 213.
(29) Goldner, Ph.; Pelle, F. *J. Lumin.* **1994**, *60*−*61*, 651.
(30) Gharavi, A.; McPherson, G. L. *J. Opt. Soc. Am. B* **1994**, *11*, 913.
(31) McPherson, A. M.; McPherson, G. L. *Solid State Commun.* **1981**, *37*, 501.
(32) Meyer, G.; Morss, L. R., Eds. *Synthesis of lanthanide and actinide compounds*; Kluwar Academic Publishers: Boston, MA, 1991.
(33) Meyer, G.; Dötsch, S.; Staffel, T. *J. Less Common Met.* **1987**, *127*, 155.
(34) This branching ratio was calculated using $(k_{CR} + k_D)/k_F$ (see Table 1) and assumes that the intrinsic relaxation from $^5D_3$ and $^5D_4$ is largely radiative.
(35) This branching ratio was calculated using k_D/k_F (see Table 1) and assumes that the intrinsic relaxation from $^5D_3$ and $^5D_4$ is largely radiative.